Novel architecture of MEMS microphone that employs deflecting micro beams and piezoresistive nano gauges

J. Czarny[a,b], T. Verdot[a], E. Redon[b], A. Walther[a], H. Lhermet[a], B. Desloges[a], K. Ege[b], P. Robert[a] et J.-L. Guyader[b]

[a]CEA LETI, 17, rue des Martyrs, 38054 Grenoble, France

[b]INSA Lyon - Laboratoire Vibrations Acoustique, 25 bis, avenue Jean Capelle, 69621 Villeurbanne, France

jaroslaw.czarny@cea.fr

Electret microphones dedicated to consumer electronics and medical applications (hearing aids) have reached the miniaturization limits. Since the release of the first microphone based on silicon micromachining, electret microphones are constantly replaced by MEMS microphones. The following paper present the novel MEMS microphone architecture that is developed in the frame of the ANR MADNEMS project. It uses micro beams that deflect in the plane of the base wafer. Signal transduction is achieved by piezoresistive nanogauges integrated in the microsystem and attached to the micro beams. Acoustic pressure fluctuations lead to the deflection of the micro beams which produces a stress concentration in the nano gauges. Such architecture enables us to reduce the surface of the deflecting element and leads to a microphone with a smaller footprint that preserves at the same time high performance.
Accurate simulations of the discussed transducer couple acoustic, mechanical and electric behavior of the system. Due to micrometric dimensions of acoustic vents, thermal and viscous boundary layers have to be taken into account. Additionally the influence of backspace volume on pressure response has to be examined. The paper will initially present general principle of operation then the coupled microphone model will be briefly presented. Afterwards we introduce technological process and finally we will focus on the microphone characterization method based on impedance tube.

1 Introduction

MEMS (Micro Electro Mechanical Systems) microphones use Silicon that provides exceptional mechanical characteristics [1] along with good electric properties and mature fabrication technology [2]. Regardless of the transduction principle (capacitive, piezoresistive, piezoelectric, optical), all of the MEMS microphones reported in the state of the art literature are based on a membrane deflecting out of the plane of the base wafer. Numerous surface micromachined membranes have been reported, among them those made of metalized silicon nitride [3, 4], the combination of silicon nitride and polysilicon [5], polysilicon [4, 6] and bulk micromachined membrane reported by Y. Iguchi [7]. Most of the reported microphones and all of the commercially available MEMS use capacitive transduction [8]. Downscaling of capacitive microphones is problematic, since the sensitivity depends on capacitance value. Moreover capacitive sensors suffer of high sensitivity to parasitic capacitance and nonlinearity.
The drawbacks of capacitive detection may be overcome with use of piezoresistive properties of Silicon nanowires. Unlike the classical piezoresistors integrated into silicon membrane, suspended nanowires do not suffer of leakage current. Further improvement of piezoresistive detection is possible since the longitudinal piezoresistive coefficient rises inversely proportional to nanowire section. Advantages of nanowire piezoresistive detection are employed in so-called M&NEMS technology developed at CEA-LETI. M&NEMS technological platform has been already successfully used for inertial sensors fabrication [2] and possibility of MEMS microphone fabrication is currently investigated.

2 Principle of operation

2.1 System architecture

Presented MEMS (fig. 1) has overall dimensions of 1.5x1.5x0.6 mm^3, it consists of 4 micro-beams placed between the inlet vents that guide the sound waves and outlet vents connected to back cavity (fig. 2). On the occurrence of sound, pressure fluctuations propagates through inlet vent and reach the diaphragm which deflects proportionally to the pressure difference between inlet and outlet vents ($\Delta p = p_1 - p_2$). Longitudinal stress induced by the motion of a beam inside suspended piezo resistive Si gauges is

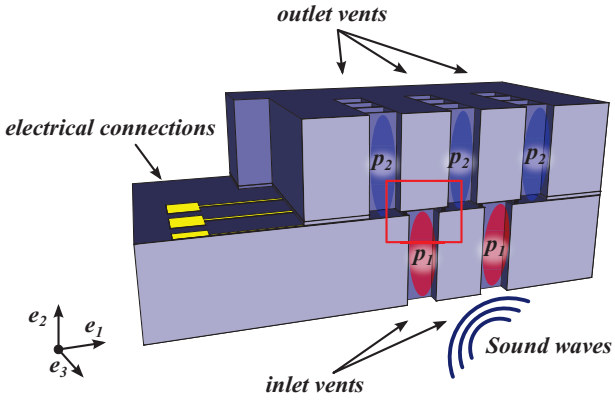

Figure 1: Cross-sectional scheme of the microphone with acoustic configuration and sensing elements.

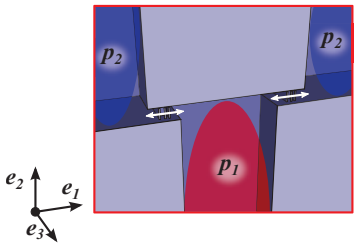

Figure 2: Focus on a coupler. White arrows indicate position and in-plane displacement for two of four microstructures.

transduced into resistance variations and measured by use of full Wheatstone bridge architecture [9] described further on figure 7. One side of each beam is attached to Si substrate through flexible hinge while the other side is free to ensure rotational movement (fig. 3).

2.2 Crucial role of thermoviscous effects

Dimensions of designed microphone ranges from 1 mm down to 1 µm. The smallest acoustic elements are the slits situated above and below the beam (fig. 4). Their dimensions $a = 1\mu m$ and $b = 2\mu m$ are much smaller than the thicknesses of thermal and viscous boundary layers (illustrated on fig. 5) for the targeted sensor bandwidth (70Hz to 10kHz) [10, 11].

Detailed analytical and FEM models that investigates thermoviscous effects have been prepared within the M&NEMS microphone project and presented in [12, 13]. Using a simplify model for moving beams, these models

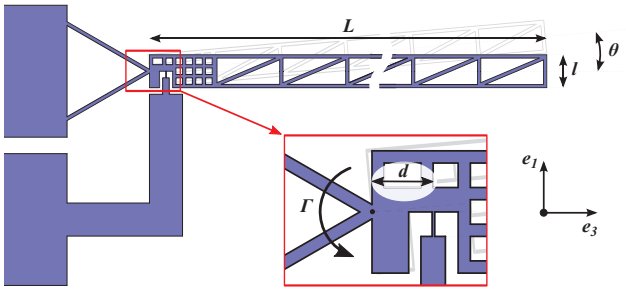

Figure 3: Top view and dimensions of single mechanical structure. Focus shows an arrangement of hinge and nanogauge.

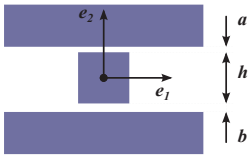

Figure 4: Dimensions of couplers (not to scale).

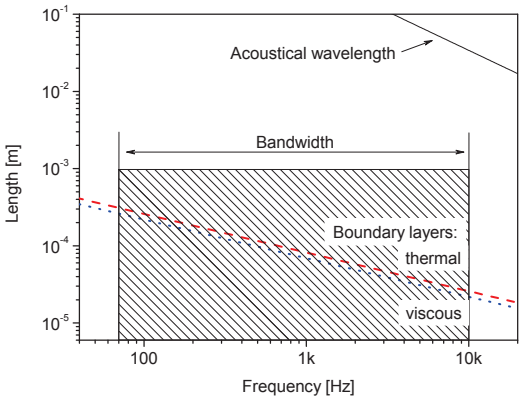

Figure 5: Acoustic wavelength and thickness of thermal and viscous boundary layers as a function of a frequency [11]. Hatched rectangle indicates the dimensions of CEA-LETI sensor.

handle fluid-structure interactions. Figure 6 focus on harmonic solutions (pressure fluctuations and velocity field) computed at 1 kHz and 12 kHz with viscothermal acoustic FEM. This solutions highlight two types of behavior: at low frequency when velocity of a beam remains weak air velocity in the slits is mainly governed by the prescribed difference of pressure (velocity profile is similar to the Poiseuille parabolic flow). In the vicinity of mechanical resonance of a structure (12 kHz), beam velocity affects air velocity in the slits and the velocity field become similar to the Couette flow, which profile is linear. These studies [12, 13] prove that viscous effects occurring in the small slits generate and maintain a pressure drop across the beams.

3 Transduction chain

Knowing that viscous effects assure that M&NEMS microphone architecture is able to efficiently transduce acoustic pressure fluctuations, we have prepared simplified model of transduction chain based on widely used lumped

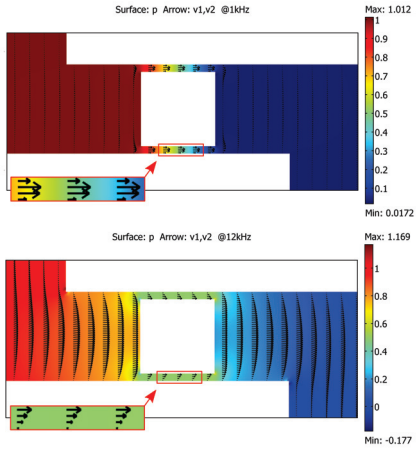

Figure 6: Pressure and velocity fields in coupler [13].

element approximation [4, 8].

3.1 Acoustical transfer function

Our considerations assume that the air is non compressible in the slits above and below beam structures. Moreover for audible bandwidth inertial effects can be neglected. Including viscous shear stress in the air, Navier-Stokes momentum balance equation provides relationship between the pressure p and velocity u fields [14]:

$$\frac{\partial p}{\partial x} = \mu \frac{\partial^2 u}{\partial y^2}, \tag{1}$$

where μ is air shear viscosity. Equation 1 is integrated considering difference of pressure Δp and no-slip conditions at fluid-structure interfaces. As a result we obtain formula for volumetric air flow Q:

$$Q = \frac{1}{R_C}\Delta p + \frac{L}{2} S_d^* \dot{\theta}, \tag{2}$$

where $\dot{\theta}$ is the angular velocity of the beam (see fig. 3), R_C denotes the total viscous resistance of slits that equals:

$$R_C = \frac{12\mu l}{a^3 L + b^3 L} \tag{3}$$

and S_d^* is modified lateral surface of a beam:

$$S_d^* = (Lh)\left(1 + \frac{a+b}{2h}\right). \tag{4}$$

Torque applied to rotating beam is defined by acoustic force reduced by viscous shear damping:

$$\Gamma = \frac{L}{2} S_d^* \Delta p - D_V \dot{\theta}, \tag{5}$$

where viscous shear damping lumped coefficient D_V is:

$$D_V = \frac{\mu L^2}{3}(lL)\left(\frac{1}{a} + \frac{1}{b}\right). \tag{6}$$

3.2 Mechanical transfer function

Mechanical transmissibility of M&NEMS structures is expressed by the value of longitudinal stress in a nanogauge σ_g generated by pressure difference Δp. We

consider fluctuation of pressure at angular frequency ω and mechanical resonance of a beam at ω_0. Knowing that the beam is an oscillator with quality factor Q_V given by viscous shear damping D_V, the mechanical transfer function becomes:

$$\frac{\sigma_g}{\Delta p} = \left[\frac{S_d^*}{S_g}\right]\left[\frac{L/2}{d}\right]\frac{dK_g d}{C + dK_g d}\left[\frac{1}{1 - \left(\frac{\omega}{\omega_0}\right)^2 + \frac{1}{Q_V}\left(j\frac{\omega}{\omega_0}\right)}\right]. \quad (7)$$

Equation 7 shows that microphone based on M&NEMS technology profits of two mechanical amplification mechanisms. First amplification mechanism comes from the ratio between the modified lateral surface of a beam S_d^* and section of a nanowire S_g while the second comes from the ratio between the lever arms ($L/2d$). Stress exerted on the section of the nanogauge is related to the ratio of strain energy in the nanogauge and the overall strain energy.

3.3 Electrical transfer function

Piezoresistive effect involve change of the conductor resistance as a function of applied stress. Variation of nanogauge resistance ΔR is proportional to the longitudinal stress σ_g:

$$\Delta R = \pi_{pzr}\sigma_g R, \quad (8)$$

where π_{pzr} and R are piezoresistive coefficient of the Silicon and nominal resistance of a nanogauge respectively. Accurate measurements of ΔR can be carried out by use of electrical architecture called the Wheatstone bridge [9]. It consists of two voltage dividers connected in parallel (fig 7 a). If we polarize both voltage dividers of Wheatstone

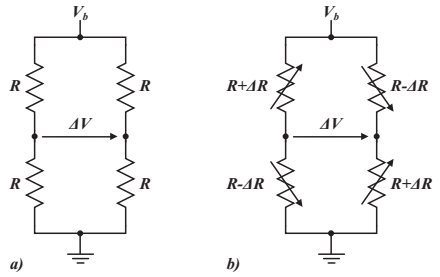

Figure 7: Wheatstone bridge architecture.

bridge with the same constant voltage V_b and we assume that the values of resistance R are perfectly matched, without stress σ_g the bridge is perfectly balanced and output voltage ΔV is null. When nanogauges are stressed (fig. 7 b), the resistance imbalance in the bridge results in output voltage ΔV. Depending on the application, one to four piezoresistors can be introduced into Wheatstone bridge architecture. In case of presented microphone the gauges are arranged into full Wheatstone bridge architecture in such manner that on the occurrence of sound pressure, two gauges are compressed while the other two are tensed (fig. 7 b). The resulting ΔV is proportional to the longitudinal stress in the nanogauge:

$$\Delta V = \left[V_b \pi_{pzr}\right]\sigma_g, \quad (9)$$

4 Sensitivity of a microphone

Sensitivity of a microphone is a resultant of its acoustical, mechanical and electrical transfer functions, however discussion of the acoustic effects has to be completed by chip-scale package construction which is an integral part of a microphone. Therefore we will introduce the influence of package and then present the total sensitivity of a microphone.

4.1 MEMS chip-scale packaging

Typical chip-scale MEMS microphone package showed on fig. 8 includes two separated chips which are MEMS and ASIC (Application-Specific Integrated Circuit). Integrated

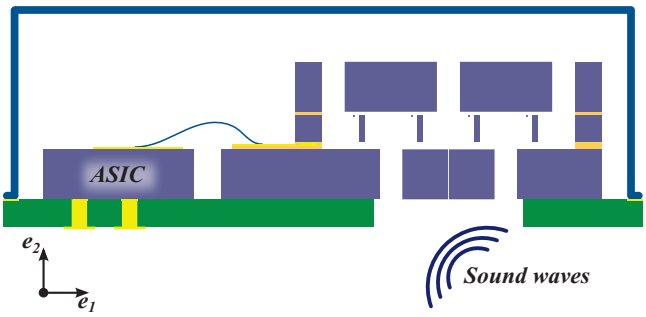

Figure 8: Bottom port configuration of MEMS microphone package (not to scale).

circuit amplifies sensor signal and furnish it in analog or digital output form. Standard PCB (Printed Circuit Board) is used as a support and metal, cup-shaped lid is used for package sealing. Depending on a sound port position we distinguish two package configurations called top and bottom port. For the M&NEMS microphone considerations bottom port configuration has been chosen.

To calculate the frequency response of the microphone, we must take into account the volume called the back cavity (obtained by deducting the volumes of the MEMS and the ASIC chips from the internal volume of a package). The volume of back cavity (V_{ar}) introduces acoustic compliance C_{ar} [10]:

$$C_{ar} = \frac{V_{ar}}{\gamma P_0}, \quad (10)$$

where γ denotes ratio of specific heats for air and P_0 is the static pressure. Regarding the closed cavity of package with dimensions larger than thermal and viscous boundary layers we can use the law of mass conservation:

$$\int_{V_{ar}} \frac{\mathrm{d}\Omega}{\gamma P_0}\frac{\partial p_{ar}}{\partial t} = \int_{V_{ar}} -\nabla \cdot v \, \mathrm{d}\Omega, \quad (11)$$

where p_{ar} is a pressure in back cavity and it equals p_2. By solving the integrals from equation 11 we obtain:

$$C_{ar}\frac{\partial p_{ar}}{\partial t} = Q_{ar}, \quad (12)$$

where Q_{ar} is a total volumetric flow entering the back cavity. For low frequencies considerations Q_{ar} equals:

$$Q_{ar} = \sum Q \approx 4\left(\frac{1}{R_C}\Delta p\right). \quad (13)$$

In harmonic mode and by replacing Δp by $p_1 - p_2$ from equations 12 and 13 we obtain acoustical transmissibility:

$$\frac{\Delta p}{p_1} = \frac{\tau j\omega}{1 + \tau\omega}, \quad (14)$$

where τ is the characteristic time constant required to restore pressure equilibrium in back cavity:

$$\tau = \frac{R_C C_{ar}}{4}. \quad (15)$$

4.2 Total sensitivity

Total sensitivity of a microphone is the assembly of its transfer functions and the acoustical transmissibility given in equation 14. For the purpose of analysis all of the components that do not depend on the frequency are gathered and expressed as S_0, the nominal sensitivity of a microphone:

$$S_0 = \left[\pi_{pzr} V_b\right]\left[\frac{S_d^*}{S_g}\right]\left[\frac{L/2}{d}\right]\frac{dK_g d}{C + dK_g d}. \quad (16)$$

The total sensitivity is a function of frequency:

$$S(\omega) = \frac{\Delta V}{p_1} = S_0\left[\frac{1}{1 - \left(\frac{\omega}{\omega_0}\right)^2 + \frac{1}{Q_V}\left(j\frac{\omega}{\omega_0}\right)}\right]\left[\frac{\tau j\omega}{1 + \tau j\omega}\right]. \quad (17)$$

Lower limit of a microphone bandwidth is fixed by the inverse of time constant $1/\tau$ coming from acoustical transmissibility. High frequency limit is set by the first mechanical resonance frequency of M&NEMS structure. Nominal sensitivity at $f = 1$ kHz and bias voltage of Wheatstone bridge $V_b = 1$ V is estimated to 5.7 mV/Pa and 6.1 mV/Pa for simplified and finite element models respectively. This value is an output voltage of Wheatstone bridge, the final sensitivity of the microphone will be enlarged by amplification of readout electronics (ASIC).

Figure 9 compares the normalized sensitivity ($\|S/S_0\|$) computed with FEM model and simple analytical model. Both transfer functions have a similar shape highlighting the high-pass filter due to acoustic behavior and high signal amplification occurring at the mechanical resonance frequency. The analytical model, which neglects the viscous effects in the vents and geometric discontinuities underestimates the viscous damping of the mechanical structure. For the same reason, the overall viscous resistance evaluated in this simple model is lower than the one evaluated in FEM model and results in an over estimation of the acoustic corner frequency.

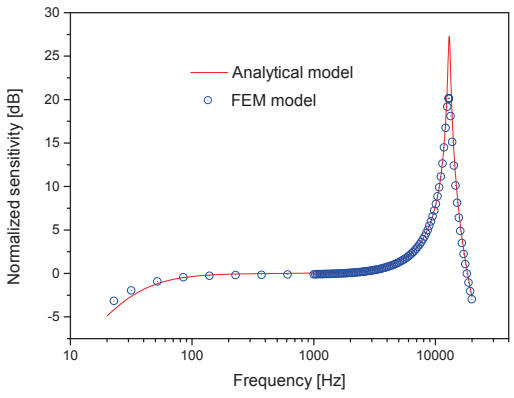

Figure 9: Normalized sensitivity of MEMS microphone.

The next natural step is to include viscosity of the vents into simplified model. However given model along with noise budgeting approach presented in [15] are already an effective way for evaluation of MEMS microphone performance.

5 Technological implementation

The MEMS fabrication is carried out in clean room with typical micro-electronic process and starts with SOI (silicon on insulator) substrate with 1 µm buried oxide and 0.25 µm Si top layer. Nanogauges of 0.25 µm width are defined by DUV (deep ultraviolet) lithography and etched by RIE (reactive ion etching). Then a 1 µm thick oxide is deposited in order to protect the gauges. Afterwards, 10 µm thick mono-crystalline Silicon is grown by epitaxy and MEMS structure is defined by DRIE (deep RIE). A cap with contact redistribution layer is bonded on top of the first wafer with eutectic bonding. Handle and cap wafers are then thinned and etched with DRIE in order to open top and bottom vents. The mechanical structure is eventually released with hydrofluoric acid vapor etching. A side view of the stack is shown on fig. 10. Described fabrication process is carried

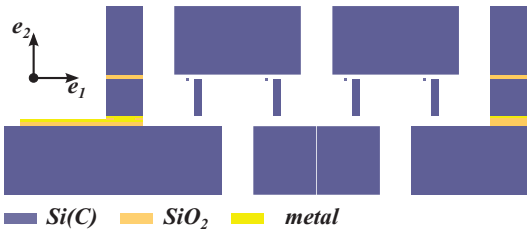

Figure 10: Side view of MEMS microphone technological implementation (not to scale).

out at CEA-LETI, most crucial technological steps including nanowires definition and MEMS etching have been already realized. Final shape of MEMS part with zoom on nanowire and rectangles indicating top (blue) and bottom (red) cavities is shown on fig. 11.

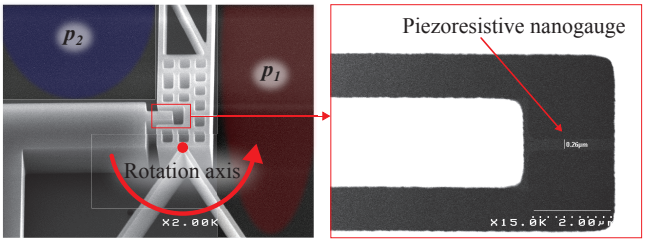

Figure 11: SEM image: top view of a microbeam and nanogauge.

6 Characterization perspective

MEMS microphones are packaged as SMT (surface mount technology) devices. Such package impose the certain problems in batch characterization. The interface for microphone may be bulky and as a consequence it can perturb the pressure field around the sensor. While most of the state of the art MEMS microphones were characterized in anechoic environment by comparison to reference microphone, we have studied the possibility of using the impedance tube [16] (fig. 12). It consist of a cylindrical

waveguide with acoustic pressure source placed at one of the extremities. For the purpose of the measurements two reference microphones were introduced to the lateral surface while the position of unknown microphone is x_m. Since the MEMS fabrication process is not finished, we have used laboratory microphone (whose sensitivity is known) to investigate the proposed measuring setup. Under condition

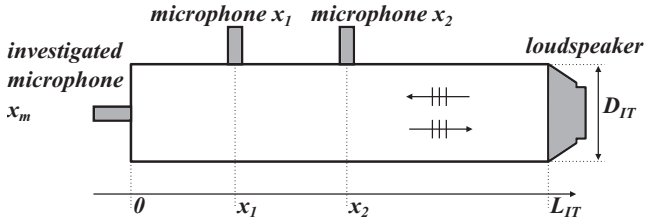

Figure 12: Sketch of functional characterization set.

of planar wave propagation and with use of Euler equation we may express the pressure ($p(x)$) and velocity ($v(x)$) fields inside the tube with use of two calibrated reference microphones. By introducing $\bar{x} = \frac{x_1+x_2}{2}$ and $h = \frac{x_2-x_1}{2}$ we obtain:

$$\begin{bmatrix} p(x_m) \\ Z_0 v(x_m) \end{bmatrix} = \frac{1}{\sin kh} \begin{bmatrix} \sin k(x_m - \bar{x}) \\ j \cos k(x_m - \bar{x}) \end{bmatrix} \frac{p_2 - p_1}{2} + \frac{1}{\cos kh} \begin{bmatrix} \cos k(x_m - \bar{x}) \\ -j \sin k(x_m - \bar{x}) \end{bmatrix} \frac{p_2 + p_1}{2}, \quad (18)$$

where x_m denotes the position of investigated microphone, Z_0 the specific impedance of air and k the wave number.

Comparison of experimental data and identified data is shown on fig. 13. Identified data obtained from equation 18

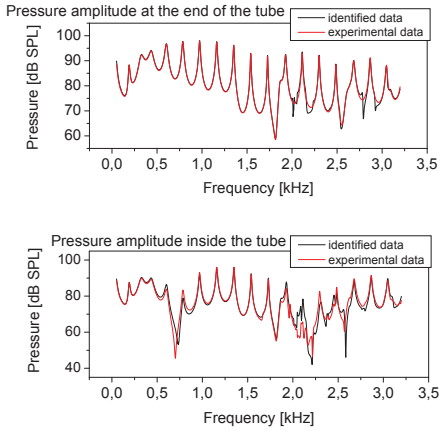

Figure 13: Comparison of experimental and identified data for impedance tube setup.

shows good match with experimental data provided by the laboratory microphone x_m situated at the end of the tube or inside the tube. However application of impedance tube for frequency response measurements is limited by its diameter (D_{IT}) and the distance between microphones x_1 and x_2:

$$f_{max} < \frac{c_0}{2D_{IT}}, \quad (19)$$

$$x_2 - x_1 < \frac{1}{2}\frac{c_0}{f_{max}}. \quad (20)$$

The first limitation concerns planar wave propagation criteria while the second one is set by the Shannon sampling theorem. For the tube used in the experiment we have observed the first radial mode of pressure propagation around 1.8 kHz.

7 Conclusion

We have proposed new architecture of MEMS microphone alternative to capacitive microphones. Employment of M&NEMS architecture offers possibility of downscaling while maintaining the sensitivity value (miniaturization of capacitive microphones is problematic since the sensitivity decrease with electrode surface).
While the MEMS fabrication is in progress, we have compared the simplified model of the microphone with viscothermal FEM. Supplementary comparison of model with M&NEMS microphone performance is needed to verify its relevance in modelisation of sensitivity, characteristic time constant, quality factor and resonance frequency of a sensor.
Presented impedance tube method allow us to designate pressure field at any point of a tube, thus depending on the electrical interface and packaging of MEMS microphone, the investigated microphone may be situated at the end or inside the tube. The method has to be still confirmed by characterization of MEMS specimen.

Acknowledgment

This work was performed within the framework of the Labex CeLyA of Université de Lyon, operated by the French National Research Agency (ANR-10-LABX-0060/ ANR-11-IDEX-0007).
Development of M&NEMS microphone is supported by the French National Research Agency (MADNEMS project ANR11-NANO-026).

References

[1] K.E. Petersen, Silicon as a mechanical material, *Proceedings of the IEEE* **70(5)**, 420-457 (1982).

[2] P. Robert, P. Rey, A. Berthelot, G. Jourdan, Y. Deimerly, S. Louwers, J. Bon, F.X. Boillot, and J. Collet, M&NEMS: a technological platform for 10-axis sensor, *SSI Conference, Amsterdam*, (2013).

[3] W. Kronast, B. Muller, W. Siedel, and A. Stoffel, Single-chip condenser microphone using porous silicon as sacrificial layer for the air gap, *Sensors and Actuators A: Physical* **87(3)**, 188-193 (2001).

[4] M.L. Kuntzman, C.T. Garcia, A.G. Onaran, B. Avenson, K.D. Kirk, and N.A. Hall, Performance and modeling of a fully packaged micromachined optical microphone, *Journal of Microelectromechanical Systems* **20(4)**, 828-833 (2011).

[5] J.W. Weigold, T.J. Brosnihan, J. Bergeron, and X. Zhang, A MEMS condenser microphone for consumer applications, *19th IEEE International Conference on Micro Electro Mechanical Systems, Istanbul*, 86-89 (2006).

[6] Chun-Kai Chan, Wei-Cheng Lai, Mingching Wu, Ming-Yung Wang, and Weileun Fang, Design and implementation of a capacitive-type microphone with rigid diaphragm and fexible spring using the two poly silicon micromachining processes, *Sensors Journal, IEEE* **11(10)**, 2365-2371 (2011).

[7] Y. Iguchi, M. Goto, M. Iwaki, A. Ando, K. Tanioka, T. Tajima, F. Takeshi, S. Matsunaga, and Y. Yasuno, Silicon microphone with wide frequency range and high linearity, *Sensors and Actuators A: Physical* **135(2)**, 420-425 (2007).

[8] A. Dehe, M. Wurzer, M. Fuldner, and U. Krumbein, The Infineon silicon MEMS microphone, *Proceedings SENSOR 2013*, 95-96 (2013).

[9] W. Kester, Practical design techniques for sensor signal conditioning, *Analog Devices Technical Reference Books*, (1999).

[10] M. Bruneau, T. Scelo, Fundamentals of Acoustics, *Wiley-ISTE*, (2006).

[11] N. Joly, Finite Element Modeling of Thermoviscous Acoustics on Adapted Anisotropic Meshes: Implementation of the Particle Velocity and Temperature Variation Formulation, *Acta Acoustica united with Acoustica* **96**, 102-114 (2010).

[12] C. Guianvarc'h, T. Verdot, J. Czarny, E. Redon, K. Ege, J.-L. Guyader, A. Walther, P. Robert, New planar nano-gauge detection microphone: analytical and numerical acoustic modeling, *21st International Congress on Acoustics, ICA 2013*, (2013).

[13] T. Verdot, C. Guianvarc'h, J. Czarny, E. Redon, K. Ege, J.-L. Guyader, Modelisation d'une architecture innovante de microphone MEMS a detection par nano jauges, *21eme Congres Francais de Mecanique*, (2013).

[14] P.Y. Kwok, M.S. Weinberg, and K.S. Breuer, Fluid Effects in Vibrating Micromachined Structures, *Journal of Microelectromechanical Systems* **14(4)**, 770-781 (2005).

[15] J. Czarny, A. Walther, B. Desloges, P. Robert, E. Redon, T. Verdot, K. Ege, C. Guianvarc'h, J.L. Guyader, New architecture of MEMS microphone for enhanced performances, *Semiconductor Conference Dresden-Grenoble (ISCDG)*, (2013).

[16] S. Lewy, Acoustique industrielle et aéroacoustique, *Hermes Science Publications* (2001).